Charge Control in Model Catalysis: The Decisive Role of the Oxide–Nanoparticle Interface
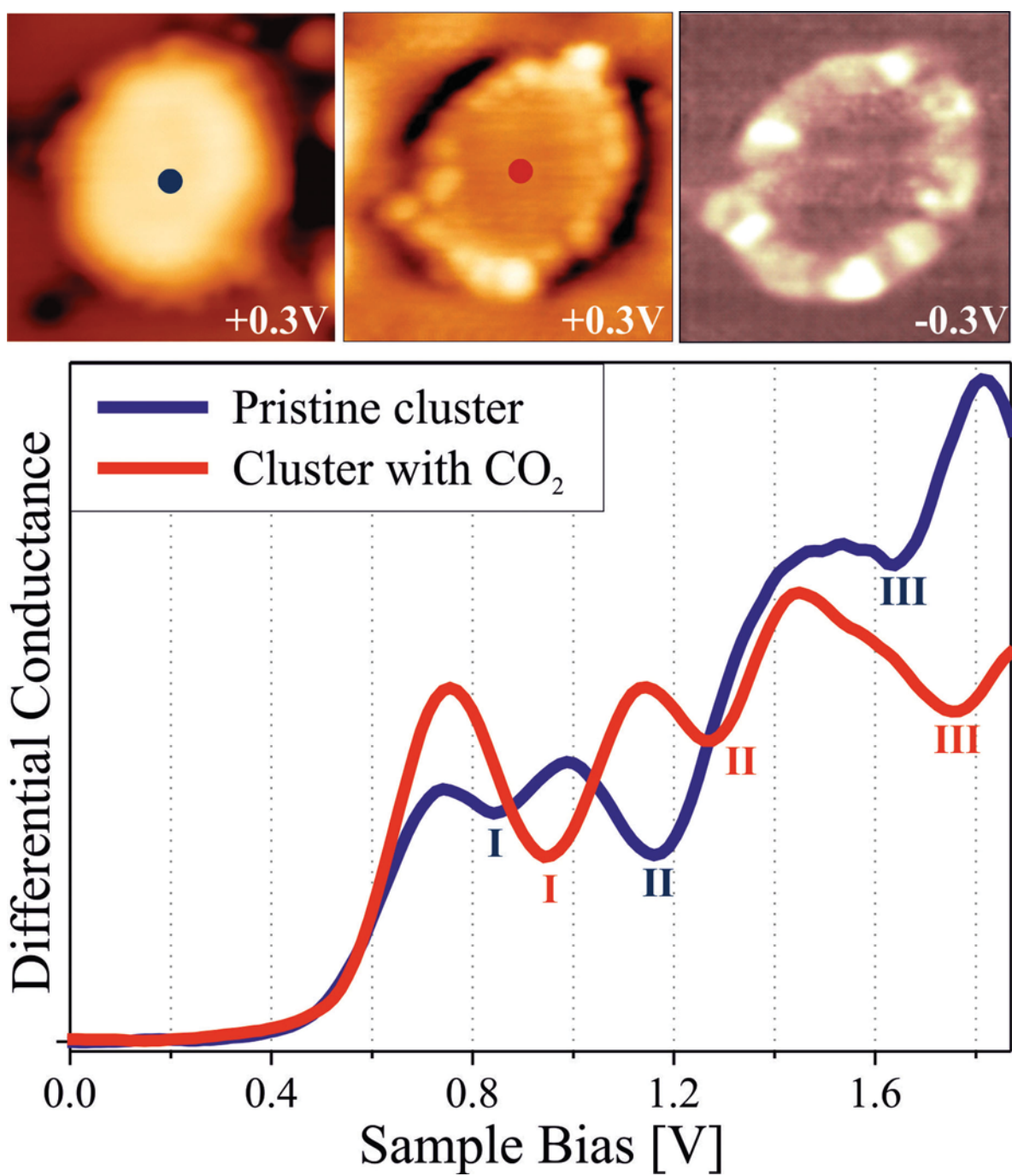
Wolf-Dieter Schneider, Markus Heyde, and Hans-Joachim Freund*[a]

Abstract: In chemistry and physics the electronic charge on a species or material is one important determinant of its properties. In the present Minireview, the essential requirements for a model catalyst system suitable to study charge control are discussed. The ideal model catalyst for this purpose consists of a material system, which comprises a single crystal metal support, covered by an epitaxially grown ultrathin oxide film, and flat, two-dimensional nanoparticles residing on this film. Several examples from the literature are selected and presented, which illustrate various aspects of electron transport from the support to the nanoparticle and vice versa. Key experiments demonstrate charge control within such model catalysts and give direct evidence for a chemical reaction at the perimeter of Au nanoparticles. The concepts derived from these studies are then taken a step further to see how they may be applied for bulk powder oxide supported nanoparticles as they are frequently found in catalytically active materials.

Introduction

Controlling the charge or the oxidation state of a species to steer its chemistry is a widely applied concept.[1] For well-defined compounds in solution or in the gas phase, there are accepted heuristic rules to assign charges to the atoms constituting the molecule based on electronegativities of the constituting atoms.[1] In some cases, it is possible to design experiments that correlate oxidation states or charges with observations. Examples are the chemical shift in X-ray photoelectron spectroscopy (XPS),[2] or spin states in electron spin resonance,[3] if appropriate theoretical modeling and an X-ray structure determination are available. When it comes to more complex systems, such as nanoparticles or clusters used in catalysis, in which a structure determination down to the atomic level is demanding, controlling the charge on such a nanoparticle or cluster is a real challenge. However, it is important to tackle this problem because knowing the charge is crucial for understanding the chemistry. There are cases reported in the literature in which the chemistry of free clusters in the gas phase, carrying positive, negative and no charge, knowing the structure and based on action spectroscopy, has been studied and pronounced differences between the acquired charge states have been identified.[4] In conjunction with computational studies, these differences may be understood and put into perspective to heuristic rules typically applied in chemistry.[5] Schwab,[6] Solymosi[7] and Vol'kenshtein[8] have addressed the influence of the support and the effect of thin oxide films on the electronic structure of supported metals and have coined the term "Electronic Theory of Catalysis". Hot electron induced chemistry, that is, electrons released through chemical reactions has also recently been discussed.[9]

In the realm of heterogeneous catalysis, in which supported nanoparticles are an important active component, charge control is even more difficult to achieve and it requires a lot more attention than dedicated to it in the past. One way to tackle this problem is to design model systems of increasing complexity, eventually capturing the situation of a real material used in a catalytic reaction,[10] yet allowing one to address charge control. A relevant design parameter for these systems is morphology, which should be chosen in such a way that scanning probe microscopy and other experimental tools, developed in the area of surface science, may be applied providing the highest level of information at the atomic scale.

In the present Minireview, we will first discuss the essential requirements for a model catalyst system suitable to study charge control. Subsequently, several examples from the published literature are selected that illustrate various aspects of electron transport within these systems. Finally, we present key experiments from our laboratory demonstrating charge control within model catalyst systems, which have measurable consequences for nanoparticle induced chemistry. The concepts derived from these studies indicate promising routes for their application in heterogeneous catalysis.

The Ultimate Model Catalyst System

To design a model catalyst system that allows us to experimentally study the issues addressed above, a number of prerequisites have to be fulfilled. Firstly and foremost, the system has to represent an oxide-supported metal nanoparticle because they are found in disperse metal catalysts. A model is schematically shown in Figure 1. Two nanoparticles are placed on a thin, epitaxially grown oxide film on a metal support.[11] The particles have different morphologies, that is, one is a three-dimensional (3D) nanoparticle, whereas the other one assumes a two-dimensional (2D) raft morphology. Depending on the materials combination, electrons may tunnel from the metal support underneath the insulating oxide film to the nanoparticle supported on top of it. This process is governed by the energy it takes to remove an electron from the interface between the metal support and the thin oxide film (ionization potential of the interface), as well as by the energy released by placing one (or several) electron(s) onto the metal nanoparticle on top of the oxide film (electron affinity of the metal nanoparticle). The idea is that scanning tunneling electron microscopy and spectroscopy (STM, STS) should be well suited to detect this process. In particular, inelastic electron tunneling spectroscopy (IETS) would then—under specific conditions—provide evidence for the number of electrons involved in the transfer process. Furthermore, due to the ability to spatially resolve the

[a] Prof. Dr. W.-D. Schneider, Dr. M. Heyde, Prof. Dr. H.-J. Freund
Department of Chemical Physics
Fritz Haber Institute of the Max Planck Society
Faradayweg 4–6, 14195 Berlin (Germany)
E-mail: freund@fhi-berlin.mpg.de

[iD] The ORCID number(s) for the author(s) of this article can be found under https://doi.org/10.1002/chem.201703169.
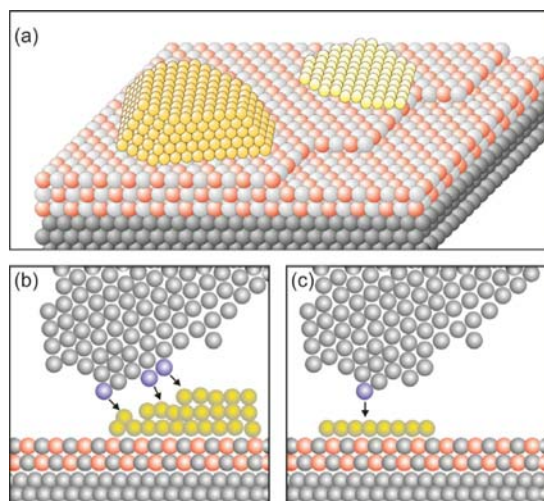
Figure 1. Schematic atomistic diagrams of two typical model catalyst systems (yellow: metal clusters, light grey and red: oxide film, gray: metal support. (a) Two nanoparticles with different morphologies (left: 3-dimensional cluster, right: 2-dimensional raft) supported on a thin oxide film, (b) scanning tunneling microscope (STM) tip (grey atoms) approaching from above the rim of the nanoparticle. The three atoms in blue at the front end and the side of the tip are responsible for the tunnel current. The black arrows indicate the tip surface interactions. Consequently, an atomically resolved topographic image of the 3D-cluster rim is difficult to obtain. (c) In contrast, the tunneling process to a well-defined 2D flat cluster is determined predominantly by the "last" atom of the tip (blue) which is closest to the flat surface. This situation allows us to obtain atomically resolved images of the whole cluster, and specifically of the cluster rim on a metal-supported thin oxide film system.

local electron density, we should be in a position to also locate where the electrons reside on the particle. Here, the morphology of the nanoparticle plays an important role. Consider the morphology of the nanoparticle with respect to the size of the tunneling tip as schematically indicated in Figure 1. It is obvious, that a 3D particle may not be imaged in its entirety at atomic resolution. STM can in principle reveal only the exact arrangement of all atoms in a nanoparticle if it is planar. For 3D nanoparticles, only the positions of the surface atoms can be mapped, whereas the atomic arrangement on the lateral facets is in most cases difficult to obtain. Nevertheless, the group of Henry achieved a complete characterization of the morphology of a 27-atom Pd nanoparticle supported on a cleaved $MoS_2(0001)$ single crystal facet.[12] The authors obtained information on the three-dimensional shape, azimuthal orientation on the substrate, and arrangement of atoms on lateral facets. So far, this is the only experiment on a small supported 3D nanoparticle, in which the number of atoms is directly obtained from the STM image. Henry and co-workers[12] compared those measurements to corresponding transmission electron spectroscopy (TEM) results, and, recently, Palmer and collaborators[13] obtained well-resolved aberration corrected TEM images of supported Au clusters and presented a route to structure determination analyzing electron beam induced transformations.

Imaging larger particles on oxide surfaces with atomic resolution using scanning probe techniques is less system-restrict-

ed. Hansen et al.[14] reported atomic resolution on supported Pd particles with a diameter larger than about 40 Å and higher than about four layers. The nanoparticles were grown on a 5 Å thick alumina film on NiAl(110). Figure 2 shows STM topographic images of such a Pd nanoparticle with atomic resolution. The top facet reveals a (111) oriented surface layer. The
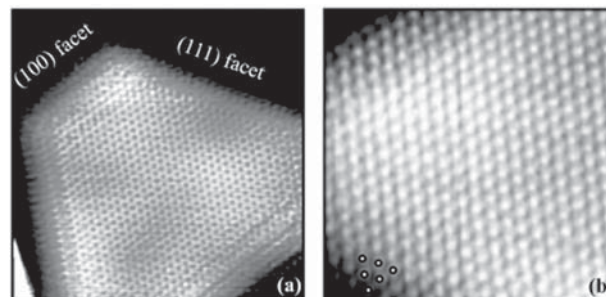

Figure 2. Atomic resolution images of crystalline nanosize Pd clusters. (a) Scan size 9.5×9.5 nm², $I_t = -0.8$ nA, $V_s = -5$ mV. (b) Scan size 4.5×4.5 nm², $I_t = -1.8$ nA, $V_s = -1.5$ mV. The resolution is kept a few layers down the sides, allowing identification of the side facets. The dots indicate atomic positions consistent with a (111) facet. Reproduced with permission from Ref. [14], copyright American Physical Society.

measured nearest neighbor distance is 2.76 ± 0.07 Å, indicating the absence of any strain in the particle [$d = 2.75$ Å; for Pd(111)]. These results show that for such particles supported on oxide surfaces it is possible to obtain atomic resolution across the entire cluster surface, although the tunneling conditions at the edge of the cluster change. In some cases atomic resolution on the largest side facets with a (111) crystallographic orientation of the particles is observed, as illustrated in the bottom part of Figure 2. The smallest particle of crystalline structure observed had a top facet of 20–30 Å widths and a height of 5–10 Å, corresponding to 2–4 atomic layers. Even adsorbates have been imaged on those top facets.[15]

Shaikhutdinov and co-workers[16] investigated strong metal-support-interaction (SMSI) states of Pt particles supported on iron oxide surfaces, which are covered with a thin FeO layer after thermal treatment. The STM images presented in Figure 3 reveal atomic resolution on the top facets and to some degree also of the side facets down to the substrate. In general, we realize that imaging the perimeter is difficult, simply because the size of the tip as well as the geometry of the STM setup is incompatible with the task.

In another example, Helveg et al.[17] synthesized monolayer MoS_2 nanocrystals with a width of about 30 Å on an Au(111) template. The MoS_2 nanocrystals were obtained by first growing approximately 30 Å wide Mo particles on the Au(111) template and subsequent sulfidation in a H_2S atmosphere. Atom-resolved STM images reveal that the small nanocrystals exhibit triangular morphology in contrast to bulk MoS_2. Figure 4 depicts an atomically resolved STM image of such a monolayer triangular nanocrystal.

The observed protrusions are arranged with hexagonal symmetry and an average interatomic spacing of 3.15 ± 0.05 Å.
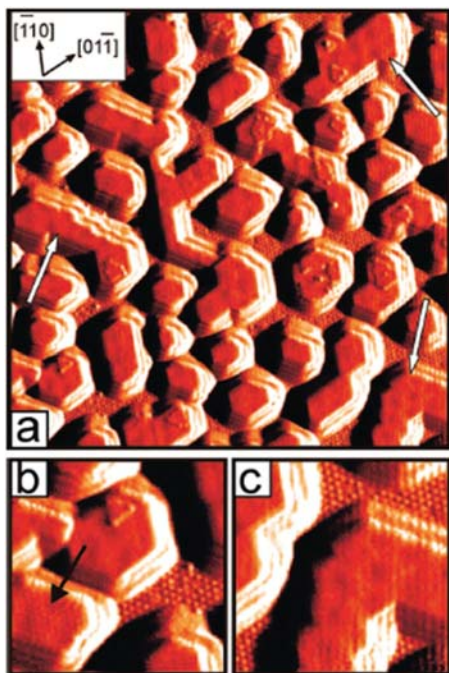
Figure 3. STM topographic images of 3D Pt clusters (covered with a thin FeO layer after thermal treatment), in which part of the descending terraces at the cluster rim are resolved. (a) STM image (scan size 80×80 nm^2, $I_t = 0.6$ nA, $V_s = \_0.5$ V) of 1.8 monolayer (ML) Pt/Fe$_3$O$_4$(111) exposed to 540 Langmuir (L) at 500 K and flashed to 850 K in ultra-high vacuum (UHV). The arrows indicate some of the top facets in which the moiré superstructure is clearly observed, as enlarged in image c. The Pt particle exhibiting a structure of about 0.6 nm periodicity is shown in image b (scan size 20×20 nm^2). Reproduced with permission from Ref. [16], copyright American Chemical Society.
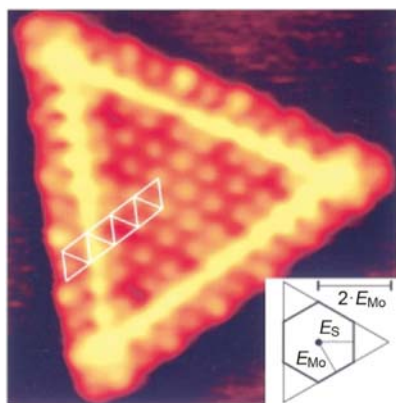

Figure 4. An atom-resolved STM image (scan size 4.1×4.1 nm^2, $I_t = 1.28$ nA, $V_t = 5.2$ mV) of a triangularly shaped single-layer MoS$_2$ nanocluster. The grid shows the registry of the edge atoms relative to those in the basal plane of the MoS$_2$ triangle. The inset shows a Wulff construction of the MoS$_2$ crystal. E_{Mo} and E_S denote the free energy for the Mo and S edges, respectively (reproduced with permission from Ref. [17], copyright American Physical Society). The lines of highly increased contrast following the edges of the MoS$_2$ triangles were shown to originate from one-dimensional metallic edge states in MoS$_2$.[18]

This is consistent with the interatomic spacing of S atoms in the (0001) basal plane of MoS$_2$. From the apparent height of only 2.0 ± 0.3 Å, the authors conclude that the MoS$_2$ nanocrys-

tals are present as single layers on the Au surface. The triangular shape of the monolayer crystals is in contrast to the expected hexagonal morphology of multilayer MoS$_2$. This implies that one of the edge terminations is considerably more stable. To answer which edge structure is more stable, the edge structures of the triangles were investigated with atomic resolution. The S atoms at the edges were found to be out of registry with the S atoms in the hexagonal lattice of the basal plane and are shifted by half a lattice constant along the edge. A comparison with density functional theory (DFT) calculations revealed that the observed edge structure is only obtained when the stoichiometry on the edges is changed, for example, only one S atom is bound to a Mo edge atom. Thus, these atomic resolution STM topographic images provided insights into the morphology (shape) and edge structure of MoS$_2$ nanocrystals.

The influence of the Au template on the observed electronic structure needs to be considered. In the case of MoS$_2$ on Au the interface is defined by an extended metal surface and a small sulphide particle, that is, reversed with respect to a supported metal catalyst, in which the interface is defined by an extended oxide (sulphide) support and a small metal particle. The above situation is often referred to as an "inverse catalyst", implying that the interface is the same. Obviously, however, this is not at all the case.

These examples illustrate the current status of imaging 3D nanoparticles with STM. In particular, the difficulty to image the oxide metal interface, that is, the rim of the particle. In case an increased electron density is localized at the rim, it is, however, essential to be able to study the rim properties. In contrast, the morphology of the two-dimensional (2D) particle shown in Figure 4 allows us to image the entire particle including the rim. As a conclusion of the above considerations, the choice of an ideal model catalyst comprises a material system composed of (i) a single crystal metal support, (ii) covered by an epitaxially grown ultrathin oxide, sulphide, nitride or chloride film, and (iii) 2D nanoparticles on the thin film obtained by diffusion-controlled growth.[19]

Growth and Characterization of Ultrathin Oxide Films

In a first step towards realistic model catalysts, we consider a metal single-crystal-thin-oxide-film support. Many investigations[20] have shown that thin oxide films, like MgO, CaO, TiO$_2$, or Al$_2$O$_3$ are especially suitable in their function as supports for metallic nanoparticles. When prepared under UHV conditions, they are atomically clean, which is a very important prerequisite for the investigation of their physical and chemical properties. These thin films exhibit roughly the same chemical and physical properties as their bulk analogs if grown to a certain thickness. As an illustrative example for the typical preparation procedures and surface analysis methods employed in the preparation and characterization of thin oxide films on metallic substrates, we present here the thin film growth of MgO films on Mo and on Ag single crystal surfaces.

The MgO(100) films are grown on Mo(100) by evaporating pure metallic magnesium at an oxygen pressure of 5×10^{-7} mbar. Auger electron spectroscopy (AES) measurements show a one-to-one stoichiometry of the films and the absence of carbon impurities.[20d] Typical thicknesses were about 1–10 monolayers, as determined by AES peak intensities and by XPS using the intensity attenuation of the Mo 3d core level with increasing film coverage.[21] Low energy electron diffraction (LEED) studies, taken of a typical MgO-film after a short annealing, show sharp (1×1) patterns. Multiple phonon losses observed in high resolution energy loss spectroscopy (HREELS), and the characteristic ultraviolet photoemission (UPS) from the O 2p valence band, indicate a well-ordered MgO(100) single crystal surface in good agreement with previous studies.[20e,f,22] Concerning the microscopic characterization, the morphology and the electronic structure of ultrathin MgO films epitaxially grown on Ag(001) were investigated on the atomic scale with scanning probe methods.[23] The Stranski–Krastanov growth mode of MgO leads to the formation of two-dimensional islands at submonolayer coverages, and, at higher coverages, as shown in Figure 5a, flat terraces of typically 50 nm widths. Atomic resolution images, depicted in Figure 5b, reveal the Ag(001) substrate and the MgO monolayer, in which only one type of ion is resolved. Figure 5c presents the growth model of MgO/Ag(001)[24] and illustrates the most favorable configuration: Mg-atoms occupy hollow sites, that is, they continue the Ag fcc lattice (lattice constant $a = 0.409$ nm), O-atoms occupy on top sites. The Ag(001) surface unit cell is indicated.[23,25]

Differential conductance measurements on ultrathin MgO films reveal that the electronic structure of three atomic layer of MgO already corresponds closely to one of the MgO(001)
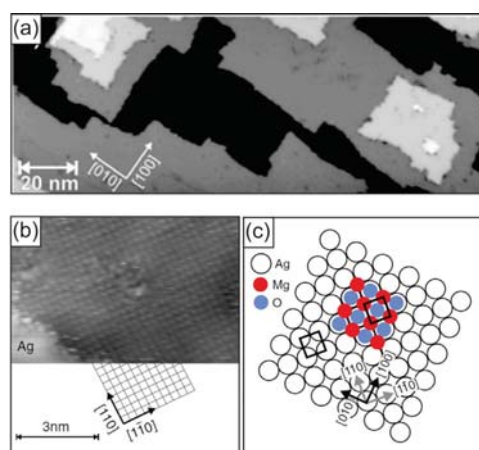
single crystal surface showing a band gap of nearly 6 eV. Calculations of the local density of states (LDOS) based on DFT with the generalized gradient approximation (GGA) support the experimental results. Within this broad energy window, the local electronic structure of supported nanoparticles can be studied by STS, opening new perspectives for the local investigation of model catalysts.[23] Recently, by careful after-growth-treatment in addition to the usual growth parameters, that is, crystal temperature, metal flux, and oxygen pressure, Pal et al.[27] succeeded to tune the morphology of the MgO film from irregular, nanometer-sized, monolayer-thick islands to larger, squared bilayer islands and to extended monolayers limited only by substrate steps. Concerning the morphology of the interface between the ultrathin MgO film and the Ag(001) substrate, a combined STM and atomic force microscopy (AFM) study revealed steps and kinks in the insulator-metal interface, a result which is not possible to obtain by STM alone.[28]

The electron trapping properties of structural elements, such as point defects, line defects, and grain boundaries, has been of a greater interest in recent years.[29] Studies on the growth behavior of MgO on Mo(001) have shown that the lattice mismatch between MgO and the Mo(001) substrate leads to the formation of line defects in the oxide to minimize tension, making this sample system ideal to study the influence of line defects on the local electronic structure.[30] The importance of electron trapping sites in MgO has already been studied with MgO/Ag(001) for point defects by Sterrer et al.[31] They are supposed to be involved in electron transfer processes on the surface. These point defects are oxygen vacancies, known as color centers, and are therefore referenced in the literature as F centers originating from the German word "Farbe". Depending on their charge state they are marked as F^0, F^+ or F^{2+}, having two, one or no electron trapped. Such electrons in the color centers can be transferred to adsorbates such as Au atoms.

The defect-free MgO surface is quite inert whereas a defect rich surface shows a high and complex chemical reactivity.[32] To understand possible reaction pathways, a detailed characterization of color centers is highly desired. Information about their local position and thus coordination, electronic structure, local contact potential and possible adsorbate interaction are of fundamental interest (Figure 6). From calculations, it has been proposed that color centers are directly involved in chemical reactions[33] for example, as adsorption sites due to more attractive defect-adsorbate interactions compared with the pristine MgO surface.

Considering that the intrinsic defect density of the film is very small, color centers need to be generated by operating the microscope in the STM mode at high currents and high sample voltages. Clean and well-grown MgO areas have been selected to ensure defined conditions beforehand. The produced defects are then preferentially located at kinks and corners of step edges (see Figure 6b). This means defect sites with a lower coordination number are preferred. In the first place, it is unknown which type of color center is imaged on the MgO surface. To gain further insight into the nature of the color centers, it is necessary to perform high-resolution Kelvin probe force microscopy (KPFM) (Figure 6d) measurements in

Figure 5. (a) STM topographic image of a 2.0 monolayer (ML) film of MgO on Ag (001), exposing MgO terraces of up to 4 ML. $I_t = 1.0$ nA, $V_t = 3.0$ V. (b) Atomic resolution indicating the lattice orientation of the substrate. ($I_t = 2$ pA, $V_t = 30$ mV). Comparable atomic resolution of an MgO film surface has been achieved by AFM.[26] (c) Growth model of MgO/Ag(001). Illustration of the most favorable configuration: Mg-atoms occupy hollow sites, that is, they continue the Ag fcc lattice (lattice constant $a = 0.409$ nm), O-atoms occupy on top sites. The Ag(001) surface unit cell is indicated. Reproduced with permission from Ref [23], copyright American Physical Society and Ref [25], copyright IOP Publishing.
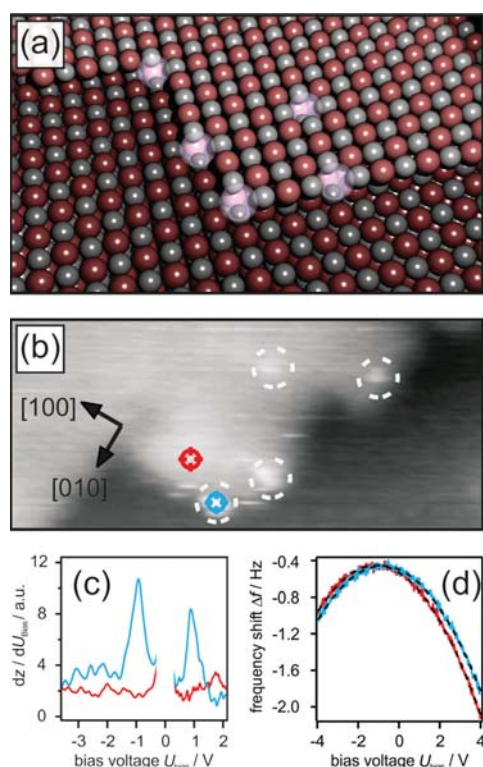
Figure 6. Spectroscopy on point defects. (a) Schematic representation of the color centers in the MgO lattice at different terrace, step edges, kinks and corner sites. (b) AFM image of 21 nm × 9 nm measured at a frequency shift of $\Delta f = -1.6$ Hz, an oscillation amplitude of $A_{osc} = 0.34$ nm and $V_S = -50$ mV. Defects are indicated by circles. The position of the spectroscopy in (c) and (d) is indicated by red and blue. (c) STS on MgO. There are no states in the MgO-film (red), whereas electronic defect states (blue) at approximately 1 and -1 V exist. (d) Frequency shift versus sample voltage spectroscopy shows a quadratic dependence at the MgO film (red) and at the defects (blue). The maxima are at different sample voltages, that is, point of different work functions.[35].

combination with scanning tunneling spectroscopy (STS; Figure 6c) at single point defect resolution. It was possible to investigate the color centers on the MgO surface in detail and to classify their charge state.[34] This demonstrates once again the great benefit of AFM and KPFM in combination with STM and STS.

The final step to obtain a realistic model nanocatalyst, is the creation of metallic nanoparticles on these ultrathin dielectric films. There are two main approaches, (i) diffusion controlled growth of 2D nanoparticles on the thin film after physical vapor deposition of the chosen metal,[19a–d] and (ii) deposition of size-selected clusters obtained by laser vaporization in He-atmosphere or, for example, by high-energy Xe-ion sputtering of the chosen metal, and subsequent mass selection in a quadrupole mass filter.[20d, 36] Below we review attempts to address model catalyst systems following the ideas outlined above.

Electron Transfer in These Model Catalyst Systems

A number of systems have been investigated. They range from individual atoms to chains of atoms and 2D rafts on insulating

films (oxides, chlorides, sulphide and nitride). The rafts encompass metal as well as oxide and sulfide aggregates. We analyze these systems with respect to the question of how charge transfer is controlled by the aggregate and the interface between it and the support.

Before experimental evidence had been presented, predictions based on computational studies for individual metal atoms on oxide films were published. In 1999, the first studies by Jennison and collaborators[37] on Pd atoms on alumina surfaces revealed strong binding upon electron transfer from the metal atom to the oxide forming a positively charged Pd atom. In contrast, Pd atoms on MgO(100) surfaces, according to Neyman et al.,[38] are relatively weakly bound and do not carry a charge. Subsequently, Nilius et al.[39] published a study on Pd on a thin alumina film grown on NiAl(110) indicating that the properties of the Pd atoms depend on the adsorption sites, without providing clear evidence on the charge state. In 2004, Repp et al.[40] published a scanning probe study on individual Au atoms on a thin NaCl layer grown on Cu(100) and Cu(111) surfaces. The well-resolved STM images allowed identification of the adsorption site of the metal atom. Even more importantly, applying voltage pulses to the tip, the Au adatom could be reversibly switched between a neutral Au^0 and a negatively charged Au^- state, as shown in Figure 7.
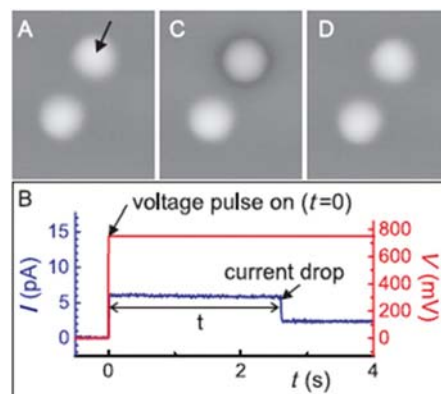

Figure 7. Example of the manipulation of the Au adatom state. After recording the image (A), the STM tip was positioned above one of the Au adoms (arrow) and a positive voltage pulse was applied to the sample. After a time t, a sharp decrease in the tunneling current can be observed (B). A subsequent STM image (C) shows that the manipulated Au adatom has a different appearance but did not change its position. By applying a negative voltage pulse, one can switch the manipulated adatom back to its initial state (D). Reproduced with permission from Ref. [40], copyright The American Association for the Advancement of Science

Their experimental results were corroborated by DFT calculations. Subsequently, a similar combined experimental and theoretical study by Olsson et al.,[41] reported that individual Ag adatoms on ultrathin NaCl films supported on Cu single crystal surfaces were manipulated by voltage pulses to acquire three different stable charge states—neutral, negatively, and positively charged adatoms. Figure 8 illustrates that the different charge states of the Ag adatoms can be distinguished by their image contrast. We note that charge switching of individual adsorbed Au and Ag adatoms on ultrathin NaCl films on
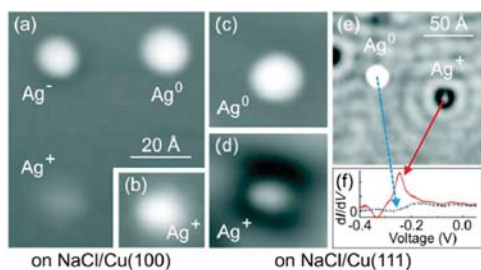
Figure 8. STM images and spectra of different Ag adatom states (Ag^0, Ag$^+$, and Ag$^-$) on NaCl(2ML)/Cu(100) [(a) and (b)] and Cu(111) [(c)–(f)]. In (a) and (c), the maximum scale (white) corresponds to a height of $=0.25$ nm; (b) and (d) show Ag$^+$ with the contrast being 4 times higher. An image at even higher contrast (e) and local dI/dV spectra (f) show scattering of interface-state electrons and an interface localization at Ag$^+$ but not at Ag^0. The solid, dashed, and dotted spectrum refers to Ag$^+$, Ag^0, and bare NaCl/Cu, respectively. The bias and the tunneling currents are (a) $V_s = 50$ mV, $I_t = 1$ pA; (b) $V_s = 200$ mV, $I_t = 0.5$ pA; (c) $V_s = -558$ mV, 62 pA; (d) $V_s = -211$ mV, 62 pA; (e) $V_s = 15$ mV, $I_t = 0.8$ pA. Reproduced with permission from Ref. [41], copyright American Physical Society.

Cu(111) had also been achieved later by using combined STM and AFM.[42] Another intriguing aspect of charged adatoms is their charge-state-dependent diffusion, found very recently for Au adatoms on these ultrathin insulating NaCl films.[43]

In 2007, Sterrer et al.[44] presented STM results on Pd atoms in comparison to Au atoms adsorbed on well-defined MgO(100) films revealing negatively charged Au atoms and neutral Pd atoms in full agreement with predictions by Pacchioni et al.[45] The metal atoms reside on the surface, with the adsorption site depending on the charge state. Negatively charged metal atoms reside on the oxygen ions, positively charged atoms reside on the Mg atom within the substrate. A study of Au and Pd atoms on a two-layer FeO(111) film on Pt(111)[46] indicates that while Pd atoms basically remain neutral, Au atoms on this substrate are positively charged. This charge and adatom dependent adsorption behavior for the two different ad-atoms is illustrated in Figure 9 for the above addressed case of Pd and Au adsorption on MgO(100). Although the Pd atoms exhibit a random arrangement on the surface, including the formation of Pd clusters and particles, the deposited Au atoms are characterized by a distribution dominated by repulsion between positively charged atoms, which seem to bind to a specific site on the surface. Infrared
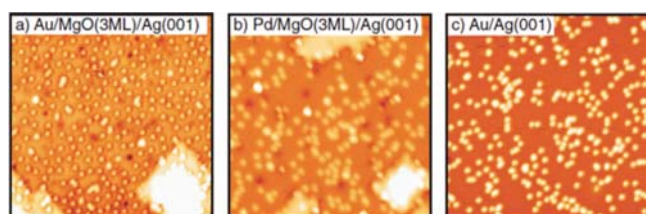

Figure 9. STM images (30×30 nm^2) of (a) Au atoms ($\theta = 2.9\%$ ML Au) adsorbed on 3 ML thin MgO films, ($V_s = 0.5$ V, $I_t = 11$ pA); (b) Pd atoms ($\theta = 2.3\%$ ML Pd) adsorbed on 3 ML thin MgO films, ($V_s = 0.2$ V, $I_t = 13$ pA); (c) Au atoms ($\theta = 2.9\%$ ML Au) adsorbed on bare Ag(001), ($V_s = 0.1$ V, $I_t = 100$ pA). Reproduced with permission from Ref. [44], copyright American Physical Society.

studies on individual adsorbed metal atoms as well as particles using CO as a probe molecule indicate charge on the metal atoms by characteristic shifts in the CO-stretching frequencies.

Individual metal atoms have also been incorporated into oxide films. A first example was reported on Pd atoms residing in a silica layer grown on Mo(112).[47] However, in this case, the interaction with the Mo substrate influences the properties. Lievens and collaborators[44] investigated the substitution of Co atoms into a NaCl film and found that the transition metal atoms may substitute, both, chlorine as well as sodium ions, assuming either a negative or a positive charge. Even the magnetic interactions between neighboring metal atoms were investigated and correlated with DFT calculations.

A series of studies on larger aggregates have been reported. The first report to experimentally count the number of electrons in a linear metal aggregate was reported by Nilius et al.[49] together with computational studies by the Sauer group in 2008. As shown in Figure 10, the important feature
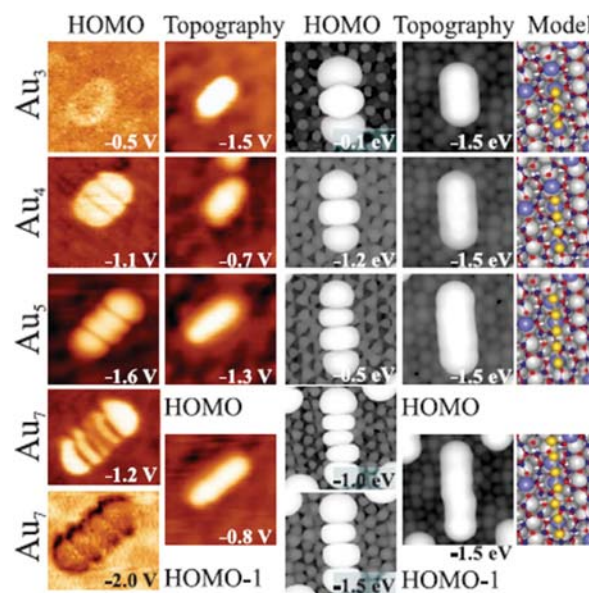

Figure 10. Experimental and calculated HOMO (highest occupied molecular orbital) shapes, topographies, and model structures for Au$_3$, Au$_4$, Au$_5$, and Au$_7$ chains. Images are 5.0×5.0 nm^2 in size. For the Au$_7$ chain, in addition the HOMO-1 is shown. Measured chain lengths are 0.9, 1.2, 1.5, and 2.2 nm; calculated distances between first and last chain atoms amount to 0.53, 0.78, 1.05, and 1.55 nm. To compare theoretical to experimental lengths, 0.2–0.3 nm should be added to both chain sides to account for the diffusivity of the 1D orbitals. Reproduced with permission from Ref. [49], copyright American Physical Society.

here is the observation of patterns in the dI/dV spectroscopic images that represent the quantum states of the system as a function of the tunneling voltage. Identifying the highest occupied and lowest unoccupied states of the chain, and knowing the number of atoms in the chain, permits to count the number of electrons provided by the Au 6s electrons.

The idea is to use the concept of a particle-in-a-box and the number of nodes in the wave functions as a function of energy. The result in case of a chain of seven Au atoms on an alumina substrate is that three electrons have been transferred

to the Au chain in addition to the electrons provided by the Au atoms in the chain. A similar analysis has been presented by Lin et al.[50] for two-dimensional aggregates (flat rafts) of Au on MgO(100). Here, the analysis, based on computations performed by the Häkkinen group, revealed patterns that were analyzed in a similar way to the linear chain yet taking into account the two-dimensional nature of the problem. The experimental and computational results for a Au_{18} nanoparticle are illustrated in Figure 11.
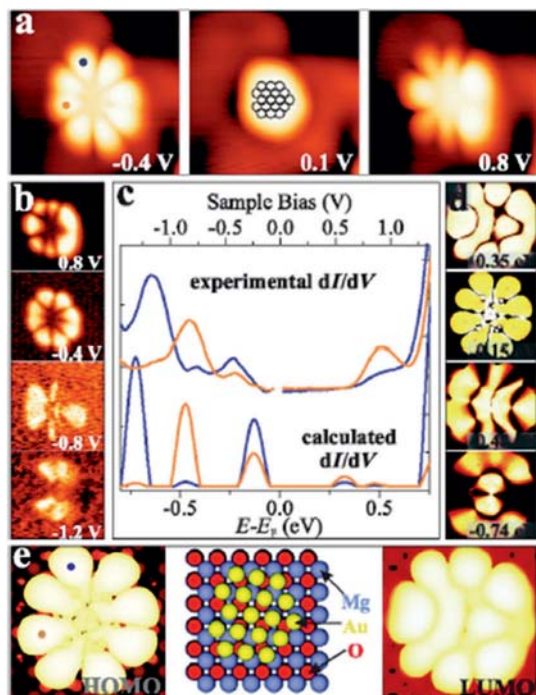

Figure 11. (a) STM topographic and (b) conductance images of an Au_{18} cluster on 2 ML MgO/Ag(001) ($I_t = 5$ pA, 3.9×3.9 nm^2) in comparison with simulated (d) conductance and (e) topographic images (2.0×2.0 nm^2) and a structures model. (c) Experimental and simulated dI/dV spectra taken at the blue and orange dots marked on the cluster in (a) and (e). Reproduced with permission from Ref. [50], copyright American Physical Society.

In this case, four extra electrons are transferred to the flat two-dimensional Au nanoparticle according to this analysis. Lin et al. performed studies on larger objects containing 100 atoms.[51] Here the geometry, in particular at the rim of the flat raft as shown in Figure 12a, is complex, which renders an analysis with respect to symmetry properties difficult. Still, according to the theoretical results there is charge transfer to the Au raft of about 0.2 e per Au atom. The complexity in structure expresses itself by partial localization of the additional charges at specific sites on the rim. Figure 12b, presenting filled and empty states of the Au nanoparticle, illustrates this finding. Häkkinen's calculations predict that localization happens preferentially at kink sites on the rim. There is almost a full extra electron at a kink site, and 0.5 e at each perimeter Au atom.

This appears to be an interesting find because charge localization may influence the adsorption of molecules. There are several sets of experiments in the literature concerning edge
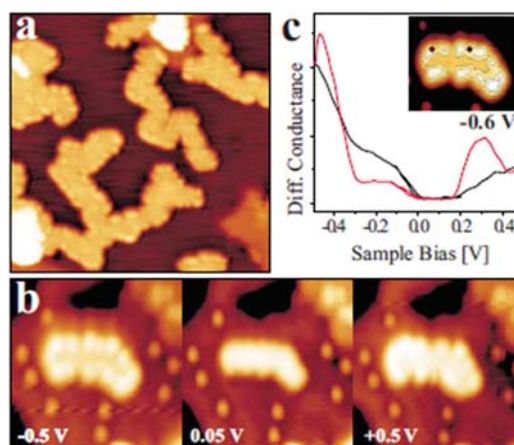

Figure 12. (a) STM topographic images of planar Au islands on 2 ML MgO/Ag(001) ($V_S = 0.2$ V, 25×25 nm^2). (b) Au island and single adatoms imaged at different bias voltages (scan size 10×10 nm^2). (c) Conductance spectra taken on a kink and a step position of the island shown in the inset. The bias set point was $+0.5$ V. The locally increased density of states at the cluster rim is clearly observed in (b) and (c) indicating the presence of a negatively charged 2D-Au cluster. Reproduced with permission from Ref. [51], copyright American Physical Society.

states on non-metallic particles. An early one came from the Besenbacher group on MoS_2 in which the authors observe edge states when those sulfide rafts are supported on an Au(111) surface[18] (see Figure 4). According to theoretical modeling these states have metallic character, and are supposed to play a key role in hydro-desulfonation reactions in catalysis. It is not clear which role the Au metal surface plays in the electronic structure of the sulfide raft. Another set of experiments has been reported on vanadium oxide particles and rafts on CeO_2(111).[52] Computational studies by the Sauer group predict a charge transfer from the vanadium atoms to the ceria surface creating highly oxidized V^{5+} species on the surface. The transferred electrons reside on the Ce ions changing their oxidation state from Ce^{4+} to Ce^{3+}.

In these two-dimensional nanoparticle systems, there is obviously no problem to observe details on the perimeter. The question is whether such observations may be transferred to three-dimensional supported particles. This is a clear challenge and so far no clear evidence has been reported. Coming back to our discussion presented in the earlier section "The Ultimate Model Catalyst System", we summarize here the existing pertinent examples. In 1999, atomically resolved images of 3d-Pd-nanoparticles supported on a thin alumina film were reported[14] (see Figure 2). Although the top facets of the particles were imaged at atomic resolution, it was not possible to clearly resolve the edge sites; some of the side facets near the top facets, however, were resolved. The Besenbacher group was able to also present images of adsorbates on the top facets.[53] Shaikhutdinov and co-workers[16] investigated Pt particles supported on iron oxide surfaces. Atomic resolution on the top facets and to some degree also of the side facets were obtained (see Figure 3). However, in general, as indicated in Figure 1, imaging the perimeter of a 3D-particle at atomic resolution is difficult, because the size of the tip as well as the

usual geometry of the STM setup are not well suited for this task.

Reactivity at the Metal-Oxide Interface and the Development of Concepts

In spite of those experimental difficulties, there are a number of combined experimental and computational studies presenting indications that the oxide-metal-interface is decisive in steering chemical reactions through charge control. Early experimental and theoretical evidence indicated charge transfer of 0.5 e from the MgO support to deposited size-selected Au_8 clusters.[54] This charge transfer turns inactive clusters into active ones in CO oxidation, opening new perspectives to tune catalytic processes on the nanoscale.

A combined theory-experimental study on Pt nanoparticles on ceria surfaces by the Libuda/Neyman groups[55] attempts to extract the transferred charge by measuring the amount of reduced ceria after deposition of the Pt particles by monitoring the Ce^{3+} signal using XPS from a film that originally did not show any reduced species as a function of Pt coverage. The claim is that this allows the authors to count the number of electrons transferred across the metal-oxide interface. The result of this effort leads to 0.12 e per Pt atom transferred from Pt to the ceria support. No direct evidence of reactions at the perimeter of nanoparticles had been presented hitherto.

Only very recently Calaza et al.[56] were able to record and image CO_2 reactivity at the rim of two-dimensional Au rafts on MgO(100). As depicted in Figure 13, in this study two important factors were exploited. On the one hand, we exploit the morphology (flat raft) of the pristine nanoparticle (Figure 13 a), which allows us to access the perimeter in detail, and on the other hand, we make use of the pronounced electron transfer towards the Au atoms residing at the perimeter, which may be used to induce chemical reactions. In the present case, CO_2 has been used as a reactant. Figure 13 b shows the Au-nanoparticle decorated with CO_2 at its perimeter, and the differential conductance spectroscopic image shown in Figure 13 c clearly reveals the increased electron density at the nanoparticle rim. CO_2 is a thermodynamically very stable molecule if no electrons are present. In the presence of electrons, CO_2 is activated by electron transfer. The energy cost to transfer an electron to CO_2 is about 0.6 eV, but if one deals with a CO_2 aggregate of at least two molecules, the electron transfer becomes energetically favorable. For a dimer, in particular, the gain is 0.9 eV as determined by molecular beam experiments in the gas phase.[56, 57]

Considering that the reaction of a CO_2 dimer to an oxalate $(C_2O_4^{2-})$ molecule has been observed on metal surfaces, which had been electron-enriched by alkali adsorption,[58] it is not surprising that the electron-rich-supported Au nanoparticles induce the formation of oxalate molecules at its perimeter at which the extra electrons are localized. According to the STM studies, the reaction is confined to the rim of the particles and the nature of the created species is confirmed by ensemble averaging infrared reflection absorption spectroscopy (IRAS), including isotopic labeling studies. When one investigates the
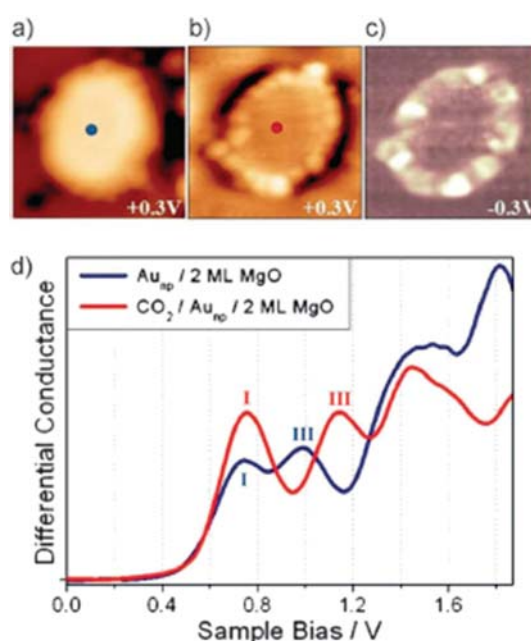

Figure 13. (a) STM topographic images of (a) a pristine planar Au cluster and (b) after exposure to CO_2, (scan size 8.0×8.0 nm², 50 pA). The Au clusters were prepared by evaporating Au on MgO mono- or bilayer films at 300 K. Subsequently the sample was exposed to 10–15 L CO_2 in a temperature range from 220–250 K. Molecules at the cluster perimeter in (b) become visible only when scanning at bias voltages between −0.5 and +0.5 V. (c) Corresponding dI/dV map, displaying the high localization of electron density at the negatively charged cluster rim. (d) dI/dV spectra taken at the center of the clusters shown in (a) (blue) and (b) (red). The positions of the first (I) and third (III) quantum well state in both spectra are indicated. Note the energy shift towards higher energy of the internal energy scale of the cluster which is compatible with a CO_2 induced decrease of the electron potential well formed by the Au island. From Ref. [56].

distribution of oxalate molecules along the perimeter one finds inhomogeneties, that may be connected to the above-mentioned inhomogeneous distribution of extra electrons along the perimeter. To look deeper into this problem we will perform IETS measurements, which will allow us to investigate the exact nature of individual molecular species and their formation.

Transfer to Real Systems

To transfer the ideas outlined above to powder systems typically applied in catalysis we need to think about systems that contain ingredients representing an electron source below the surface of an oxide, which may be exploited to charge a supported nanoparticle on top of the surface. A natural choice is the use of transition-metal dopants, which may replace cations in the support oxide, for example Mg in MgO or Ca in CaO. These dopants should then be designed to allow for an easy change of the oxidation state, thereby releasing electrons that may be taken up by metal nanoparticles forming on the surface. Experimentally, this has been realized by placing Mo dopants into a CaO lattice exposing the (100) surface.[59] At a concentration of 1–2 % of Mo, the nanoparticles at the surface all assume flat raft morphologies, observed for the thin film sys-

tems discussed above.[60] Au on CaO with Mo-dopants[62] or Au on MgO on Ag(100)[61] both result in 2D Au rafts. In the first case, the transferred electrons are delivered by the Mo impurities, in the second one by electrons tunneling from the Ag substrate through the oxide film to the Au nanoparticle. It should be possible to perform studies on chemical reactions in a similar way. It is interesting to ask how the particles on the surface communicate with the dopants underneath the surface. Is it tunneling or is it another mechanism? We have some indications that phonons may be involved in the electron transfer process.[62]

We emphasize here again that the formation of planar Au islands on top of the ultrathin MgO and CaO insulating films has itself its origin in the charge transfer from the substrate to the Au nanoparticle.[45,63] Upon charge transfer from the Au raft to the adsorbed CO_2 molecules at its perimeter, the quantum well states in the 2D Au nanoparticles are shifted in energy.[61b] This effect reveals how molecular adsorption influences individual quantum systems, a topic of utmost relevance for heterogeneous catalysis.

Conclusions

Two-dimensional nanoparticle rafts are ideally suited to investigate the connection between cluster charges and chemical reactivity, an aspect of particular importance in catalysis. Metal-supported thin oxide film systems provide a platform to develop concepts on how charge may be exchanged between the support, the nanoparticle, and reactive molecules residing on the nanoparticle. The dielectric films decoupling the nanoparticle from the support are essential for the application of scanning probe methods which enable us to study and to elucidate the distribution of charge on the nanoparticle. The concepts developed here may be transferred to real catalyst systems by replacing the electron source represented by the metal support in the case of thin film systems by appropriate dopants in the case of bulk oxide materials.

Conflict of interest

The authors declare no conflict of interest.

Keywords: catalysis · charge transfer · microscopy · nano particles · scanning probe · surface science

[1] F. A. Cotton, G. Wilkinson, *Advanced Inorganic Chemistry*, Wiley, Hoboken, **1972**.
[2] K. Siegbahn, *ESCA applied to free molecules*, North-Holland Pub. Amsterdam, **1970**.
[3] M. Brustolon, E. Giamello. (eds.), *Electron Paramagnetic Resonance: A Practitioner's Toolkit*, Wiley, Hoboken, **2009**.
[4] P. Gruene, D. M. Rayner, B. Redlich, A. F. G. v. d. Meer, J. T. Lyon, G. Meijer, A. Fielicke, *Science* **2008**, *321*, 674–676.
[5] D. J. Harding, A. Fielicke, *Chem. Eur. J.* **2014**, *20*, 3258–3267.
[6] G. M. Schwab, K. Koller, *J. Am. Chem. Soc.* **1968**, *90*, 3078–3080.
[7] F. Solymosi, *Catal. Rev. Sci. Eng.* **1968**, *1*, 233–255.
[8] F. F. Vol'kenshtein, *Russ. Chem. Rev.* **1966**, *35*, 537.
[9] J. Y. Park, L. R. Baker, G. A. Somorjai, *Chem. Rev.* **2015**, *115*, 2781-2817.
[10] H. J. Freund, N. Nilius, T. Risse, S. Schauermann, *Phys. Chem. Chem. Phys.* **2014**, *16*, 8148–8167.
[11] H.-J. Freund, *J. Am. Chem. Soc.* **2016**, *138*, 8985–8996.
[12] A. Piednoir, E. Perrot, S. Granjeaud, A. Humbert, C. Chapon, C. R. Henry, *Surf. Sci.* **1997**, *391*, 19–26.
[13] Z. W. Wang, R. E. Palmer, *Phys. Rev. Lett.* **2012**, *108*, 245502.
[14] K. H. Hansen, T. Worren, S. Stempel, E. Lægsgaard, M. Bäumer, H. J. Freund, F. Besenbacher, I. Stensgaard, *Phys. Rev. Lett.* **1999**, *83*, 4120–4123.
[15] K. Højrup Hansen, Ž. Šljivančanin, E. Lægsgaard, F. Besenbacher, I. Stensgaard, *Surf. Sci.* **2002**, *505*, 25–38.
[16] Z. H. Qin, M. Lewandowski, Y. N. Sun, S. Shaikhutdinov, H. J. Freund, *J. Phys. Chem. C* **2008**, *112*, 10209–10213.
[17] S. Helveg, J. V. Lauritsen, E. Lægsgaard, I. Stensgaard, J. K. Nørskov, B. S. Clausen, H. Topsøe, F. Besenbacher, *Phys. Rev. Lett.* **2000**, *84*, 951–954.
[18] M. V. Bollinger, J. V. Lauritsen, K. W. Jacobsen, J. K. Nørskov, S. Helveg, F. Besenbacher, *Phys. Rev. Lett.* **2001**, *87*, 196803.
[19] a) J. A. Venables, J. H. Harding, *J. Cryst. Growth* **2000**, *211*, 27–33; b) G. Haas, A. Menck, H. Brune, J. V. Barth, J. A. Venables, K. Kern, *Phys. Rev. B* **2000**, *61*, 11105; c) C. R. Henry, *Surf. Sci. Rep.* **1998**, *31*, 231–326; d) L. Piccolo, C. Becker, C. R. Henry, *Eur. Phys. J. D* **1999**, *9*, 415–419; e) R. Franchy, *Surf. Sci. Rep.* **2000**, *38*, 195.
[20] a) M. Bäumer, H.-J. Freund, *Prog. Surf. Sci.* **1999**, *61*, 127–198; b) M. Frank, M. Bäumer, R. Kühnemuth, H.-J. Freund, *J. Phys. Chem. B* **2001**, *105*, 8569–8576; c) S. C. Street, D. W. Goodman, (Eds.: D. A. King, D. P. Woodruff), Elsevier, Amsterdam, **1997**, Vol. 8, p. 375; d) U. Heiz, F. Vanolli, L. Trento, W. D. Schneider, *Rev. Sci. Instrum.* **1997**, *68*, 1986; e) M. C. Wu, J. S. Corneille, C. A. Estrada, J.-W. He, D. W. Goodman, *Chem. Phys. Lett.* **1991**, *182*, 472–478; f) M. C. Wu, J. S. Corneille, J. W. He, C. A. Estrada, D. W. Goodman, *J. Vac. Sci. Technol. A* **1992**, *10*, 1467–1471; g) X. Shao, P. Myrach, N. Nilius, H.-J. Freund, *J. Phys. Chem. C* **2011**, *115*, 8784.
[21] M. H. Schaffner, F. Patthey, W. D. Schneider, *Surf. Sci.* **1998**, *417*, 159–167.
[22] a) M. Liehr, P. A. Thiry, J. J. Pireaux, R. Caudano, *Phys. Rev. B* **1986**, *33*, 5682–5697; b) L. H. Tjeng, A. R. Vos, G. A. Sawatzky, *Surf. Sci.* **1990**, *235*, 269–279; c) J.-W. He, P. J. Møller, *Chem. Phys. Lett.* **1986**, *129*, 13–16; d) J.-W. He, P. J. Møller, *Surf. Sci.* **1986**, *178*, 934–942; e) J.-W. He, P. J. Møller, *Surf. Sci.* **1987**, *180*, 411–420; f) I. Alstrup, P. J. Møller, *Appl. Surf. Sci.* **1988**, *33–34*, 143–151.
[23] S. Schintke, S. Messerli, M. Pivetta, F. Patthey, L. Libioulle, M. Stengel, A. De Vita, W.-D. Schneider, *Phys. Rev. Lett.* **2001**, *87*, 276801.
[24] a) U. Schönberger, O. K. Andersen, M. Methfessel, *Acta Metall. Mater.* **1992**, *40*, S1–S10; b) C. Li, R. Wu, A. J. Freeman, C. L. Fu, *Phys. Rev. B* **1993**, *48*, 8317–8322; c) E. Heifets, E. A. Kotomin, R. Orlando, *J. Phys. Condens. Matter* **1996**, *8*, 6577.
[25] S. Schintke, W. D. Schneider, *J. Phys. Condens. Matter* **2004**, *16*, R49–R81.
[26] M. Heyde, G. H. Simon, H.-P. Rust, H.-J. Freund, *Appl. Phys. Lett.* **2006**, *89*, 263107.
[27] a) J. Pal, M. Smerieri, E. Celasco, L. Savio, L. Vattuone, M. Rocca, *Phys. Rev. Lett.* **2014**, *112*, 126102; b) J. Pal, M. Smerieri, E. Celasco, L. Savio, L. Vattuone, R. Ferrando, S. Tosoni, L. Giordano, G. Pacchioni, M. Rocca, *J. Phys. Chem. C* **2014**, *118*, 26091–26102.
[28] S. Baumann, I. G. Rau, S. Loth, C. P. Lutz, A. J. Heinrich, *ACS Nano* **2014**, *8*, 1739–1744.
[29] a) K. P. McKenna, A. L. Shluger, *Phys. Rev. B* **2009**, *79*, 224116; b) H. M. Benia, P. Myrach, A. Gonchar, T. Risse, M. Nilius, H. J. Freund, *Phys. Rev. B*

2010, *81*, 241415; c) S. Stuckenholz, C. Büchner, M. Heyde, H.-J. Freund, *J. Phys. Chem. C* **2015**, *119*, 12283 – 12290.

[30] a) S. Benedetti, P. Torelli, S. Valeri, H. M. Benia, N. Nilius, G. Renaud, *Phys. Rev. B* **2008**, *78*, 195411; b) S. Benedetti, F. Stavale, S. Valeri, C. Noguera, H.-J. Freund, J. Goniakowski, N. Nilius, *Adv. Funct. Mater.* **2013**, *23*, 75 – 80.

[31] M. Sterrer, M. Heyde, M. Novicki, N. Nilius, T. Risse, H. P. Rust, G. Pacchioni, H. J. Freund, *J. Phys. Chem. B* **2006**, *110*, 46 – 49.

[32] G. Pacchioni in *Theory of point defects at the MgO surface, Vol. 9* (Ed. D. P. Woodruff), Elsevier, Amsterdam, **2001**, pp. 94 – 135.

[33] a) A. M. Ferrari, G. Pacchioni, *J. Phys. Chem.* **1995**, *99*, 17010 – 17018; b) E. Scorza, U. Birkenheuer, C. Pisani, *J. Chem. Phys.* **1997**, *107*, 9645 – 9658.

[34] a) T. König, G. H. Simon, H. P. Rust, G. Pacchioni, M. Heyde, H. J. Freund, *J. Am. Chem. Soc.* **2009**, *131*, 17544 – 17545; b) T. König, G. H. Simon, U. Martinez, L. Giordano, G. Pacchioni, M. Heyde, H.-J. Freund, *ACS Nano* **2010**, *4*, 2510 – 2514.

[35] T. König, G. H. Simon, L. Heinke, L. Lichtenstein, M. Heyde, *Beilstein J. Nanotechnol.* **2011**, *2*, 1 – 14.

[36] a) U. Heiz, W. D. Schneider, *Crit. Rev. Solid State Mater. Sci.* **2001**, *26*, 251 – 290; b) P. Fayet, F. Granzer, G. Hegenbart, E. Moisar, B. Pischel, L. Wöste, *Phys. Rev. Lett.* **1985**, *55*, 3002 – 3004.

[37] A. Bogicevic, D. R. Jennison, *Phys. Rev. Lett.* **1999**, *82*, 4050.

[38] K. M. Neyman, S. Vent, N. Rösch, G. Pacchioni, *Top. Catal.* **1999**, *9*, 153 – 161.

[39] N. Nilius, T. M. Wallis, W. Ho, *Phys. Rev. Lett.* **2003**, *90*, 046808.

[40] J. Repp, G. Meyer, F. E. Olsson, M. Persson, *Science* **2004**, *305*, 493 – 495.

[41] F. E. Olsson, S. Paavilainen, M. Persson, J. Repp, G. Meyer, *Phys. Rev. Lett.* **2007**, *98*, 176803.

[42] L. Gross, F. Mohn, P. Liljeroth, J. Repp, F. J. Giessibl, G. Meyer, *Science* **2009**, *324*, 1428 – 1431.

[43] J. Repp, W. Steurer, I. Scivetti, M. Persson, L. Gross, G. Meyer, *Phys. Rev. Lett.* **2016**, *117*, 146102.

[44] M. Sterrer, T. Risse, U. Martinez Pozzoni, L. Giordano, M. Heyde, H.-P. Rust, G. Pacchioni, H.-J. Freund, *Phys. Rev. Lett.* **2007**, *98*, 096107.

[45] G. Pacchioni, L. Giordano, M. Baistrocchi, *Phys. Rev. Lett.* **2005**, *94*, 226104.

[46] L. Giordano, G. Pacchioni, J. Goniakowski, N. Nilius, E. D. L. Rienks, H.-J. Freund, *Phys. Rev. Lett.* **2008**, *101*, 026102.

[47] S. Ulrich, N. Nilius, H.-J. Freund, U. Martinez, L. Giordano, G. Pacchioni, *Phys. Rev. Lett.* **2009**, *102*, 016102.

[48] Z. Li, H. Y. T. Chen, K. Schouteden, K. Lauwaet, L. Giordano, M. I. Trioni, E. Janssens, V. Iancu, C. Van Haesendonck, P. Lievens, G. Pacchioni, *Phys. Rev. Lett.* **2014**, *112*, 026102.

[49] N. Nilius, M. V. Ganduglia-Pirovano, V. Brázdová, M. Kulawik, J. Sauer, H. J. Freund, *Phys. Rev. Lett.* **2008**, *100*, 096802.

[50] X. Lin, N. Nilius, H. J. Freund, M. Walter, P. Frondelius, K. Honkala, H. Häkkinen, *Phys. Rev. Lett.* **2009**, *102*, 206801.

[51] X. Lin, N. Nilius, M. Sterrer, P. Koskinen, H. Häkkinen, H.-J. Freund, *Phys. Rev. B* **2010**, *81*, 153406.

[52] M. Baron, H. Abbott, O. Bondarchuk, D. Stacchiola, A. Uhl, S. Shaikhutdinov, H.-J. Freund, C. Popa, Maria V. Ganduglia-Pirovano, J. Sauer, *Angew. Chem. Int. Ed.* **2009**, *48*, 8006 – 8009; *Angew. Chem.* **2009**, *121*, 8150 – 8153.

[53] J. V. Lauritsen, M. Nyberg, R. T. Vang, M. V. Bollinger, B. S. Clausen, H. Topsøe, K. W. Jacobsen, E. Lægsgaard, J. K. Nørskov, F. Besenbacher, *Nanotechnology* **2003**, *14*, 385.

[54] a) A. Sanchez, S. Abbet, U. Heiz, W. D. Schneider, H. Häkkinen, R. N. Barnett, U. Landman, *J. Phys. Chem. A* **1999**, *103*, 9573 – 9578; b) B. Yoon, H. Häkkinen, U. Landman, A. Wörz, J.-M. Antonietti, S. Abbet, K. Judai, U. Heiz, *Science* **2005**, *307*, 403 – 407.

[55] Y. Lykhach, S. M. Kozlov, T. Skala, A. Tovt, V. Stetsovych, N. Tsud, F. Dvorak, V. Johanek, A. Neitzel, J. Myslivecek, S. Fabris, V. Matolin, K. M. Neyman, J. Libuda, *Nat. Mater* **2016**, *15*, 284 – 288.

[56] F. Calaza, C. Stiehler, Y. Fujimori, M. Sterrer, S. Beeg, M. Ruiz-Oses, N. Nilius, M. Heyde, T. Parviainen, K. Honkala, H. Häkkinen, H.-J. Freund, *Angew. Chem. Int. Ed.* **2015**, *54*, 12484 – 12487; *Angew. Chem.* **2015**, *127*, 12661 – 12665.

[57] a) A. Stamatovic, K. Stephan, T. D. Märk, *Int. J. Mass Spectrom. Ion Processes* **1985**, *63*, 37 – 47; b) E. L. Quitevis, D. R. Herschbach, *J. Phys. Chem.* **1989**, *93*, 1136 – 1139; c) R. N. Compton, P. W. Reinhardt, C. D. Cooper, *J. Chem. Phys.* **1975**, *63*, 3821 – 3827.

[58] F. M. Hoffmann, M. D. Weisel, J. A. K. Paul in *Characterization of CO_2 Adsorption and Reaction on Single Crystal Metal Surfaces*, Woodhead Publishing, Cambridge, **1994**, pp. 55 – 63.

[59] Y. Cui, N. Nilius, H.-J. Freund, S. Prada, L. Giordano, G. Pacchioni, *Phys. Rev. B* **2013**, *88*, 205421.

[60] a) Y. Cui, C. Stiehler, N. Nilius, H.-J. Freund, *Phys. Rev. B* **2015**, *92*, 075444; b) X. Shao, Y. Cui, W.-D. Schneider, N. Nilius, H.-J. Freund, *J. Phys. Chem. C* **2012**, *116*, 17980 – 17984.

[61] a) C. Stiehler, Y. Pan, W.-D. Schneider, P. Koskinen, H. Häkkinen, N. Nilius, H.-J. Freund, *Phys. Rev. B* **2013**, *88*, 115415; b) C. Stiehler, F. Calaza, W.-D. Schneider, N. Nilius, H.-J. Freund, *Phys. Rev. Lett.* **2015**, *115*, 036804.

[62] Y. Cui, S. Tosoni, W.-D. Schneider, G. Pacchioni, N. Nilius, H.-J. Freund, *Phys. Rev. Lett.* **2015**, *114*, 016804.

[63] a) D. Ricci, A. Bongiorno, G. Pacchioni, U. Landman, *Phys. Rev. Lett.* **2006**, *97*, 036106; b) M. Sterrer, T. Risse, M. Heyde, H.-P. Rust, H.-J. Freund, *Phys. Rev. Lett.* **2007**, *98*, 206103; c) N. Nilius, *Surf. Sci. Rep.* **2009**, *64*, 595 – 659.
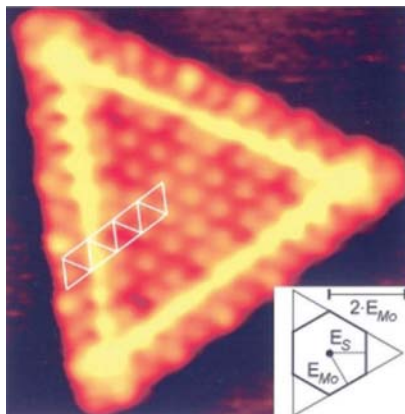
MINIREVIEW

W.-D. Schneider, M. Heyde, H.-J. Freund*

■■ – ■■

**Charge Control in Model Catalysis:
The Decisive Role of the Oxide–
Nanoparticle Interface**

Taking charge of the situation: In chemistry and physics the electronic charge on a species or material is one important determinant of its properties. In this Minireview, the essential requirements for a model catalyst system suitable to study charge control are discussed. Examples from the literature illustrate various aspects of electron transport from the support to the nanoparticle and vice versa. The concepts derived from these studies are then taken a step further to see how they may be applied for bulk powder oxide supported nanoparticles as they are frequently found in catalytically active materials.

Inducing or steering a chemical reaction by controlling the charge is a key aspect in catalysis. The charge flow at an oxide–metal interface is of paramount importance for a successful catalytic reaction. Scanning probe investigations of such an interface reveal a two-dimensional Au particle of one monolayer height and a diameter of 6 nm residing on a magnesium oxide film, the same Au raft after adsorption of CO_2 at its rim, the high localization of electron density at the negatively charged cluster rim, and the change in energy of the first quantum well states on CO_2 adsorption.